


**Three-dimensional Rashba spin splitting dominated by out-of-plane spin polarization**Rongrong Xie,<sup>1</sup> Panfeng Cao<sup>1</sup>,<sup>1</sup> Zheyuan Xu,<sup>1</sup> Boyi Xu,<sup>1</sup> Jinyue Fu,<sup>1</sup> Xiaoli Zhu,<sup>1</sup> Xianwei Fu,<sup>1</sup> Sheng-Yi Xie<sup>1,\*</sup>, Ying Jiang,<sup>1,†</sup> and Anlian Pan<sup>1,2,‡</sup><sup>1</sup>Key Laboratory for Micro-Nano Physics and Technology of Hunan Province, School of Physics and Electronics, and College of Materials Science and Engineering, Hunan University, Changsha 410082, China<sup>2</sup>Hunan Institute of Optoelectronic Integration, Hunan University, Changsha 410082, China (Received 12 December 2022; revised 28 March 2023; accepted 30 March 2023; published 28 April 2023)

Rashba-type spin-orbit coupling is a long-term active topic due to its superiority of magnetic-field-free control of the electron spin. However, numerous Rashba-related works focus on improving the magnitude of the spin splitting that exhibits the traditional in-plane spin polarization. Very few studies concern manipulating the direction of the spin splitting, such as the generation of out-of-plane spin polarization especially in nonmagnetic materials. Intriguingly, this research field has recently become very appealing owing to its great prospects in high-density and energy-efficient spintronic applications. Here, we report a prominent out-of-plane spin polarization in the two-dimensional Dion-Jacobson (DJ) perovskite and reveal that it is the physical origin of the large Rashba spin splitting observed in both experiments and theoretical calculations. Consequently, the spin-split band structures of the studied system must be interpreted by a proposed three-dimensional Rashba model, with the spin polarization mainly along the out-of-plane direction. Moreover, the temperature-dependent Rashba spin splitting shows that both static and dynamical Rashba effects contribute to the total spin splitting, where the out-of-plane spin polarization always dominates the overall splitting. Such a robust generation of this unconventional spin component indicates the significant influence of the in-plane asymmetric crystal field on the spin-orbit interactions. It is worth emphasizing that it is this out-of-plane spin splitting, not the commonly considered in-plane ones, responsible for the reported large band splitting in DJ perovskites. These results present that the studied system may serve as a type of spin source material to explore the attractive out-of-plane spin polarization, which is highly desired for high-density magnetic switching as well as field-free spin-based computing. It also suggests that crystal symmetry engineering can be a promising strategy to manipulate the spin polarization.

DOI: [10.1103/PhysRevB.107.155436](https://doi.org/10.1103/PhysRevB.107.155436)**I. INTRODUCTION**

Rashba-type spin-orbit coupling (SOC) that integrates the advantages of generation, manipulation, and detection of spin current in nonmagnetic materials has been a textbook-style mechanism in developing energy-efficient spintronics [1–5]. Owing to the interplay between SOC and spatial inversion symmetry breaking, the Rashba effect enables the generation of energy-degenerate but spin-resolved band contours in momentum ( $k$ ) space with preserved time-reversal symmetry (i.e., the so-called Rashba spin splitting) [2–4,6]. This unique feature makes Rashba systems appealing due to their ability to realize spin-to-charge interconversion via the direct or inverse Edelstein effect [7–10], which holds great promise in various spin-orbit-driven applications such as efficient magnetization switching [11–13], spin-based logics [14–19], and spintronic terahertz emitters [20,21], thus substantially flourishing the emerging area called *spin-orbitronics* [22].

Nowadays Rashba spin splitting occurs in a wide variety of systems and heterostructures [6,23–32]. Most of them conform to the traditional two-dimensional (2D) Rashba model with the spin splitting and spin-momentum locking along the in-plane momentum directions, due to the out-of-plane inversion asymmetry of the confining potential [3]. Much Rashba-related research focuses on improving the magnitude of the spin splitting, while very few studies concern manipulating the direction of the spin splitting [24,33–36]. This leaves a still rarely explored yet intriguing question of whether an out-of-plane Rashba spin splitting is universal due to the in-plane symmetry breaking of the crystal field. More than 10 years ago, a sizable out-of-plane spin-polarization component was evidenced responsible for the giant Rashba spin splitting in the surface alloy Bi/Ag(111) [24], although similar investigations were very scarce since then [33–36]. However, with the big data era arriving and energy-conservation targets, the exploration of out-of-plane spin polarization has recently fascinated the science community and quickly entered the field of spin-orbitronics, owing to its great potential in realizing high-density and low-power-consumption magnetic memories with perpendicular magnetizations [37–56]. Conventional in-plane spin-momentum locking can only switch the adjacent parallel, not perpendicular, magnetizations via

\* shengyi\_xie@hnu.edu.cn

† jying@hnu.edu.cn

‡ anlian.pan@hnu.edu.cn

spin-orbit torques. Although the out-of-plane spin polarization for perpendicular switching could be induced by applying an external magnetic field to break the in-plane symmetry [37,50], the energy-efficient field-free switching is more desirable for practical applications. This fosters the exploration of symmetry-reduced materials with broken in-plane symmetry [49,57,58] or the use of ferromagnets/noncollinear antiferromagnets [39,41,43–46,48,51,53,55,56] to generate the demanding out-of-plane spin polarization. So far, such studies are still few and in their early stages.

Perovskites as promising candidates for next-generation photovoltaics have recently been shown as a kind of strong Rashba material [59] with the Rashba splitting energy competing with those at the top of the line [27,29–31]. The exciting aspect of perovskite-based Rashba materials is that their band gap extrema are dominated by the heavy atoms (Pb, I, etc.) with strong SOC, which results in considerable Rashba spin splitting at the band edges and makes their spin manipulation accessible by optical [60–67], electrical [68,69], and magnetic fields [70–72]. This significantly extends the perovskite-based spintronic applications including spin-optoelectronics like spin light-emitting diodes [73] as well as spin-transport devices like spin valves for magnetic switching [73,74]. Spin injection, accumulation, transport, and detection were realized in a single system with perovskite/ferromagnet interfaces [75]. Moreover, both theoretical and experimental studies demonstrated the possibility of spin-to-charge interconversion in perovskites [76,77], indicating their prospects in spin-orbitronic applications. Despite the controversial debates on the presence of the Rashba effect in three-dimensional (3D) perovskites, 2D layered perovskites have been convincing as a solid Rashba system [62,68,78–87]. Particularly, the 2D Dion-Jacobson (DJ) perovskite (AMP)PbI<sub>4</sub> [AMP = 4-(aminomethyl)piperidinium][AMP = 4-(aminomethyl)piperidinium] was found with both robust Rashba and ferroelectric effects [80,83], the two characteristics that are highly desiring for nonvolatile in-memory computing [88–91]. Further, the organic cations that bridge the octahedra interlayers in this DJ perovskite are oriented alternatively along the in-plane axes [80,92], indicating the in-plane symmetry breaking along those axes. Thereby, the layered DJ perovskite may be a good platform for exploring the out-of-plane spin polarization, which may contribute to the resulting Rashba spin splitting for potential spin-orbitronic applications. However, such investigations are still lacking at present.

In this paper, we study the Rashba spin splitting in the 2D layered DJ perovskite (AMP)PbI<sub>4</sub> by spectroscopic characterizations coupled with density functional theory (DFT) and *ab initio* molecular dynamics (AIMD) calculations. The physical origin of the observed large Rashba splitting was evidenced due to the presence of a prominent out-of-plane spin polarization in the sample. In addition, the spin-resolved band structures of this system manifested an anisotropic 3D Rashba splitting with a dominant out-of-plane spin component plus two relatively weaker in-plane ones, meaning stronger in-plane symmetry breaking is present in the studied system. This contrasts with the commonly adopted 2D Rashba model where the spin splitting occurs only within the in-plane momentum directions due to the solely out-of-plane symmetry

breaking. Moreover, the experimental and theoretical studies confirmed that both static and dynamical Rashba effects contribute to the total spin-splitting, with the out-of-plane spin polarization always prevailing in the system. These results unveil that the intrinsic in-plane crystal field is sufficient to support an out-of-plane spin polarization to affect the band structures and thus physical properties of semiconductors. Combining the advantages of flexibly structural and chemical engineering of SOC, excellent ambient stability, and easy fabrication, this system opens a playground for manipulating the interplay between the lattice, spin, and orbit degrees of freedom, holding promising potential in developing energy-efficient spintronics and spin-orbitronics.

## II. METHODS

### A. Materials synthesis

The 2D layered DJ perovskites [(AMP)PbI<sub>4</sub>] were synthesized by the aqueous solution method, as previously reported [80,92]. A mixture of AMP (57.1 mg, 0.5 mmol) and PbO (111.6 mg, 0.5 mmol) powders dissolved in concentrated hydroiodic acid (HI, 57 wt. %, 5 mL) were first put in a 20 mL flask, and then H<sub>3</sub>PO<sub>2</sub> (50 wt. %, 0.5 mL) was added. The flask was sealed and kept at 125 °C under stirring for 1 h. After that, the flask was cooled to room temperature slowly. The obtained (AMP)PbI<sub>4</sub> single crystals display orange color.

### B. Materials characterizations

The x-ray diffraction (XRD) pattern of the (AMP)PbI<sub>4</sub> was obtained using Lab XRD-6100 (45 kV, 30 mA) under Cu K $\alpha$  radiation operating in a  $2\theta$  range from 10° to 80° at room temperature. The steady-state excitation power- and temperature-dependent photoluminescence (PL) measurements as well as the circular polarization-resolved PL measurements were carried out using a confocal microscope (WITec, alpha-300) equipped with a 50 $\times$  objective lens and a 488-nm continuous wave Ar-ion laser. The helicity of the excitation laser was adjusted by a quarter-wave plate (AQWP05M-600, Thorlabs), and a razor edge long-pass 488-nm laser filter was used before detecting the PL signal by a spectrometer (UHTS300). Right ( $\sigma^+$ ) and left ( $\sigma^-$ ) circularly polarized PL components were obtained by using a quarter-wave plate and a polarizer (WP25M-UB, Thorlabs) before the detector. For temperature-dependent studies, the temperature was controlled by a continuous liquid nitrogen flow cryostat coupled with a temperature controller (ST-500, Janis Research Company).

### C. Theoretical calculations

All first-principles calculations were based on DFT which was implemented in VASP [93]. The interaction between core and valence electrons were treated with the projector augmented-wave method, whereas the electron-electron interaction was described with the PBE functional [94]. The cutoff energy for a plane-wave basis was set to 520 eV, along with a  $2 \times 2 \times 2$  Monkhorst-Pack k-point mesh for (AMP)PbI<sub>4</sub>. All structures were relaxed until the atomic forces on each ion were  $< 0.01$  eV/Å<sup>-1</sup> with the electron relaxation convergence

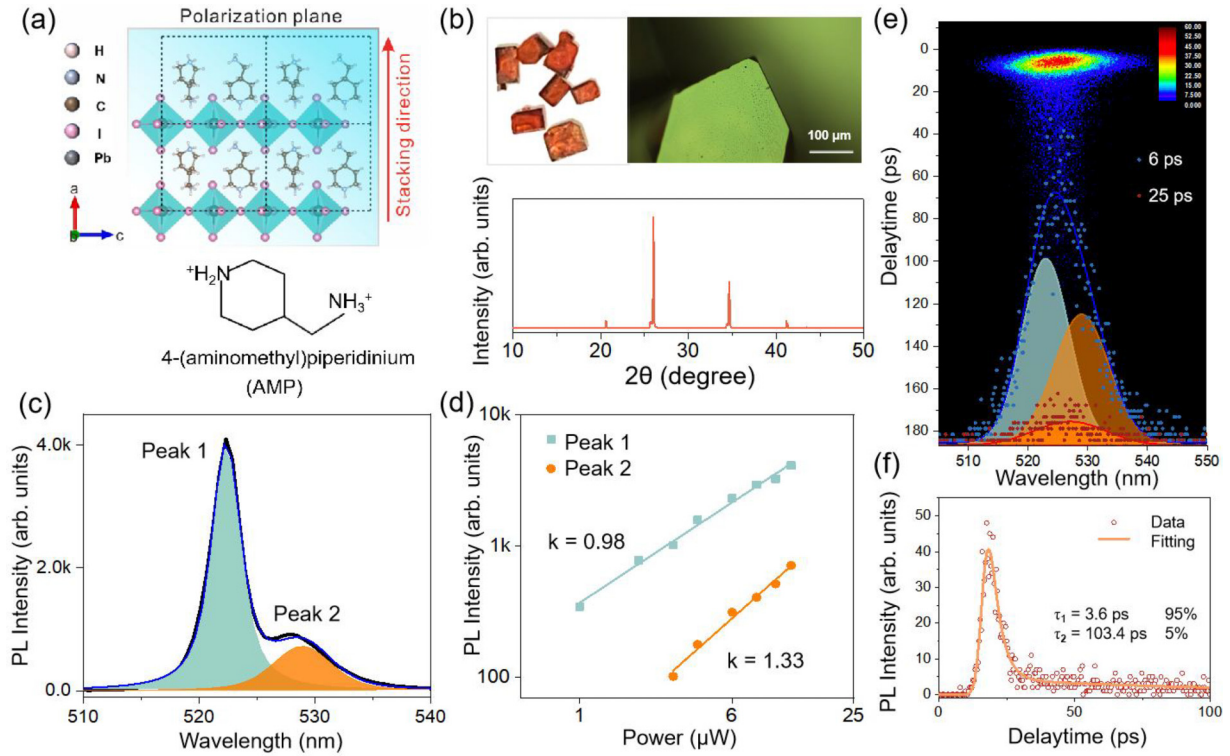


FIG. 1. (a) Schematic illustration of the crystal structure of the two-dimensional (2D) layered Dion-Jacobson (DJ) perovskite (AMP) $\text{PbI}_4$ .  $a$ ,  $b$ , and  $c$  denote the crystal axis directions. The vermilion arrow represents the stacking direction along the  $a$  axis of (AMP) $\text{PbI}_4$  single crystal. The gradient blue plane ( $a$ - $c$  plane) denotes the polarization plane of the crystal. The bottom part shows the structure of the organic AMP cation. (b) Top: Photograph (left) and optical microscopy image (right) of the synthesized (AMP) $\text{PbI}_4$  single crystals. The scale bar is  $100\ \mu\text{m}$ . Bottom: X-ray diffraction (XRD) pattern of (AMP) $\text{PbI}_4$  single crystals. (c) Steady-state photoluminescence (PL) spectrum and its component decomposition via the Gauss fitting for (AMP) $\text{PbI}_4$  at 80 K. Peaks 1 and 2 are marked by the different colors. (d) The logarithmic plots of the integrated intensity of the PL peaks ( $I_{\text{PL}}$ ) as a function of the excitation power ( $I_{\text{ex}}$ ) for (AMP) $\text{PbI}_4$  at 80 K. The solid lines are the results of fitting by the power-law relationship:  $I_{\text{PL}} \propto I_{\text{ex}}^k$  ( $k$  is the fitting parameter). (e) Streak camera image, time-resolved PL (TRPL) spectra, and their component decomposition via the Gauss fitting at 6 ps (blue dot) and 25 ps (red dot) for (AMP) $\text{PbI}_4$  at 80 K. (f) TRPL dynamics at 527 nm taken from (e) with short ( $\sim 3.6$  ps) and much longer ( $\sim 103.4$  ps) lifetime components.

criterion of  $10^{-5}$  eV in two consecutive loops. The SOC effects were considered in the calculations. Spin-energy band projections and spin textures were processed using the PyProcar program [95]. AIMD is taken on the canonical ensemble [96], with a time step of 1 fs.

### III. RESULTS AND DISCUSSION

The crystal structure of (AMP) $\text{PbI}_4$  belongs to the monoclinic system, and its space group is  $Pc$  (#7,  $C_s^2$ ) [80,83,92]. The schematic illustration of the crystal structure of (AMP) $\text{PbI}_4$  is shown in Fig. 1(a), where the inorganic layers of corner-sharing  $[\text{PbI}_6]^{4-}$  octahedra are bridged by a single layer of AMP cations via the strong hydrogen bonding interactions [92]. Note that the AMP cations are oriented alternatively with a special up and down configuration, and the stacking direction of the inorganic layers is along the  $a$  axis of the crystal [80]. The as-grown single crystals show orange color and rectangular platelike shape with lateral sizes of several millimeters [top left panel of Fig. 1(b)]. The optical microscopy image of the 2D (AMP) $\text{PbI}_4$  microplate demonstrates a relatively flat surface due to its layered structure property [top right panel of Fig. 1(b)]. The XRD pattern of

(AMP) $\text{PbI}_4$  displays sharp peaks, implying the high crystallinity of the synthesized sample [bottom panel of Fig. 1(b)]. The steady-state PL spectrum and its component decomposition via the Gauss fitting are shown in Fig. 1(c) for (AMP) $\text{PbI}_4$  at 80 K, with the main PL peak locating at 522 nm (Peak 1) and a side peak at 528 nm (Peak 2). The integrated PL intensity of these two components shows nearly linear excitation-power dependence (Figs. 1(d) and S1 in the Supplemental Material [97]), indicating their emission dominated by the exciton-type transitions, consistent with previous results [87]. Such dual PL emission has also been observed in other perovskites, where the high-energy PL component was attributed to the direct band gap transition, the low-energy one to the momentum-indirect transition due to the Rashba effect [64,100,101]. Similar assignments were made for DJ perovskites in previous works [80,86,87]. Thereby, we can tentatively ascribe the high-energy peak (Peak 1) observed here to the direct exciton transition and the low-energy peak (Peak 2) to the indirect band gap transition induced by Rashba spin splitting, which was further verified by the following time-resolved PL (TRPL) measurements via streak camera. The streak camera image that demonstrates the time evolution behavior of the PL spectrum is shown in Fig. 1(e) for



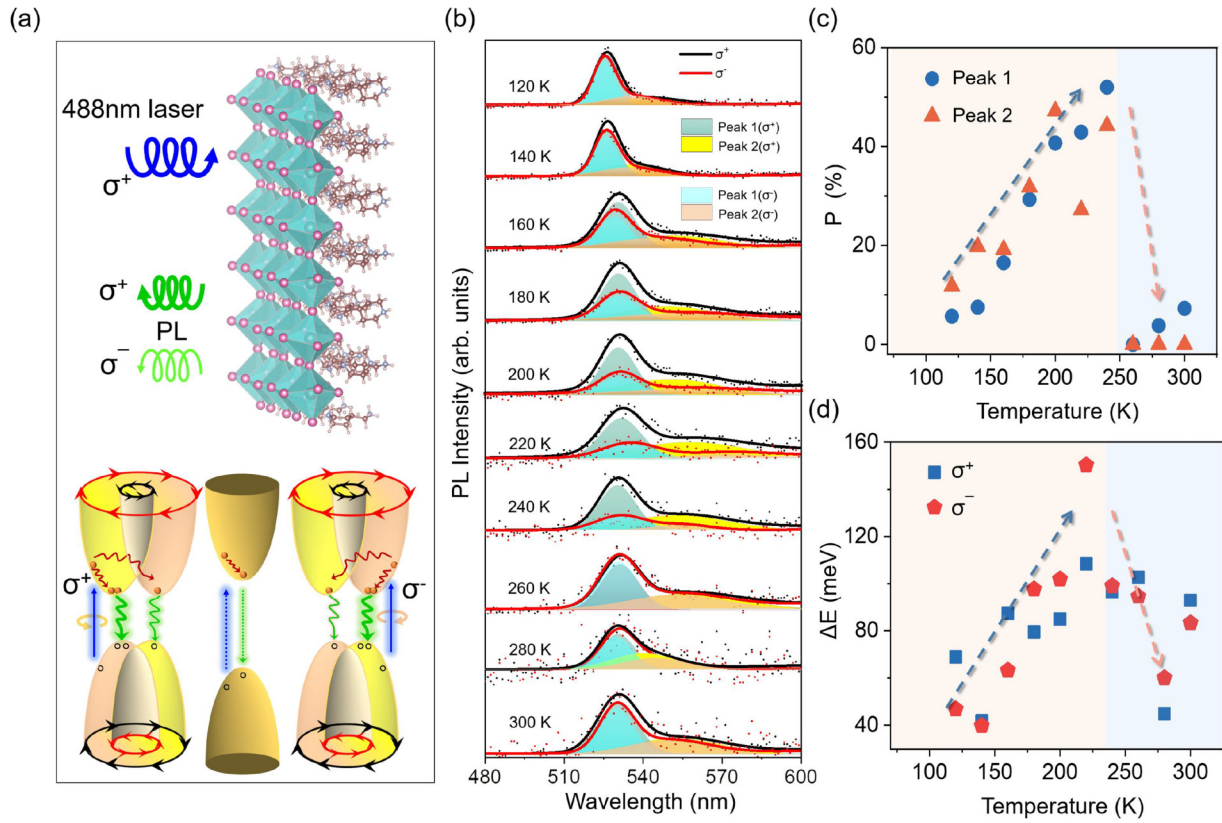


FIG. 2. (a) Schematic illustration of the Rashba spin splitting with the subbands being selectively excited by either right ( $\sigma^+$ ) or left ( $\sigma^-$ ) circularly polarized light. (b) Circular polarization-resolved photoluminescence (PL) spectra and component decompositions (Peaks 1 and 2) via the Gauss fitting for (AMP)PbI<sub>4</sub>.  $\sigma^+$  and  $\sigma^-$  represent the right (black) and left (red) circularly polarized PL spectra under the excitation of a 488-nm  $\sigma^+$  polarized laser. (c) Value of the degree of polarization ( $P$ ) for (AMP)PbI<sub>4</sub> at various temperatures. The circle represents the  $P$  value at the main peak (Peak 1), while the triangle represents that at the side peak (Peak 2). (d) Temperature-dependent energy difference ( $\Delta E$ ) between the dominant and side PL components from  $\sigma^+$  and  $\sigma^-$  circularly polarized PL spectra.

(AMP)PbI<sub>4</sub> at 80 K, from which most of the PL signal decayed within the first 10 ps, while a weak but nonnegligible PL tail persisted at longer times. The extracted PL spectra at the earlier ( $\sim 6$  ps) and later ( $\sim 25$  ps) decay times echo this phenomenon. As seen, two PL components with the dominant and side peaks at 522 and 529 nm exist in the earlier decay time, while only one weak component at  $\sim 527$  nm is left in the later decay time [see the bottom in Fig. 1(e)]. Correspondingly, the TRPL dynamics at 527 nm exhibits two lifetime components with the dominant one of  $\sim 3.6$  ps, while the minor one is much longer ( $\sim 103.4$  ps) [Fig. 1(f)]. The presence of a side PL component plus a particularly long lifetime points to the formation of a momentum-indirect band in (AMP)PbI<sub>4</sub>, as mentioned above.

To further verify the existence of Rashba spin splitting in the studied DJ perovskite, we carried out circular polarization-resolved PL measurements, which is a powerful technique widely used in examining the Rashba effect. The work principle of this technique is schematically shown in Fig. 2(a). If there is a Rashba effect, the originally spin-degenerate bands will split into two subbands with opposite spin orientations, which generally results in the momentum-direct to indirect band gap transition in the perovskites [101–103]. The energy and momentum differences between the degenerate and splitting bands are the so-called Rashba splitting energy

( $\Delta E_R$ ) and Rashba wave vector ( $k_R$ ). Since the split two bands are locked with specific spin orientations, we can selectively excite one of these bands using circularly polarized pump light. That is, if the subband with spin up can be excited by the right ( $\sigma^+$ ) circularly polarized light, then the other band with spin down could be populated by the left ( $\sigma^-$ ) circularly polarized light according to the optical selection rules. In our experiment, a  $\sigma^+$  polarized laser at 488 nm was applied to excite the perovskites, and both  $\sigma^+$  and  $\sigma^-$  polarized PL spectra were detected to check the Rashba effect. Normally, the larger the Rashba effect, the more difference between the intensity of  $\sigma^+$  ( $I^+$ ) and  $\sigma^-$  ( $I^-$ ) polarized PL emission, which can be quantitatively described by the degree of circular polarization ( $P$ ) with the definition as [104,105]  $P = 100\%(I^+ - I^-)/(I^+ + I^-)$ .

The circular polarization-resolved PL spectra with Gauss fitting and the corresponding  $P$  values within the emission window are shown in Figs. 2(b) and S2 in the Supplemental Material [97]. The existence of nonzero values of  $P$  unambiguously evidences the presence of spin-splitting bands in the band structure. Moreover, the  $P$  value shows strong temperature dependence, which increases monotonously from  $\sim 5.7\%$  at 120 K to  $\sim 52\%$  at 240 K and then drops to near zero when further increasing the peak temperature [Fig. 2(c)]. Such unusual temperature-dependent behavior was repeatable in

(AMP)PbI<sub>4</sub>. The possible origin of this phenomenon may arise from the competition between two processes, that is, the dynamical structure symmetry breaking and restoration processes. At the beginning, when the temperature starts increasing, it is well known that lattice deformation of the inorganic [PbI<sub>6</sub>]<sup>4-</sup> octahedra can occur due to the generation of longitudinal optical phonons with prominent Pb-I bending/stretching vibration motions in the perovskites [106]. This thermally assisted lattice deformation can break the structure inversion symmetry, leading to the temperature-dependent Rashba spin splitting called the dynamical Rashba effect [64,87,101,107]. The higher the temperature, the more intense the structure distortion, and thus, the larger observed  $P$  value appears. Moreover, the side PL peak [Peak 2 in Fig. 2(b)] representing the splitting band transition becomes redshifted and more prominent as the temperature increases, and the energy difference  $\Delta E$  between the main and side components increases remarkably as well (from  $\sim 40$  meV at 120 K to  $\sim 110$  meV at 240 K) [Fig. 2(d)]. However, when the temperature exceeds 240 K, the dramatic decrease of the  $P$  value indicates the structure symmetry restoration process is dominant. This is possible since the AMP molecules in this perovskite were reported to be able to rearrange their locations at higher temperature to restore the structure symmetry [80], although the transition temperature is different between this paper and the previous result. This is probably caused by the dissimilar sample conditions like thickness, defects, and surface morphology. Meanwhile, the side peak in the PL spectra beyond 240 K tends to fade away, and the energy difference  $\Delta E$  descends substantially [Fig. 2(d)], consistent with the trend of the  $P$  value [Fig. 2(c)]. Nevertheless, we cannot exclude the possibility of phase transition near this temperature to cause the almost vanished  $P$  value and the sharply dropped  $\Delta E$ . The temperature-dependent PL spectra of this perovskite was studied in another work with the investigated temperature also truncated at 250 K [86], implying the peculiarity at this temperature. Additionally, the fast spin-flip rate [61,101] and weak PL intensity at high temperature may contribute to the disappearance of the  $P$  value. These all suggest that the quantity  $P$  is a very sensitive parameter. Nonetheless, the  $P$  value observed in this paper is up to  $\sim 52\%$ , which is much higher than those reported in previous works and other perovskites [80,87,101,104]. The high  $P$  value along with the large energy difference  $\Delta E$  manifests the robust Rashba band splitting in this perovskite.

However, the physical origin responsible for the observed Rashba effect in this DJ perovskite remains ambiguous. For instance, whether it arises from the conventional out-of-plane symmetry breaking or from the unconventional in-plane symmetry breaking or both and how those broken symmetries modify the band structure, thus influencing the physical behavior of the system, are still unclear. Theoretical calculations are thereby performed to further identify the existence of the Rashba effect in the studied system as well as to clarify the related underlying mechanism in detail. The electronic band structures and projected density of states of the DJ perovskite are calculated with and without SOC (Figs. 3(a) and S3 in the Supplemental Material [97]). As seen, the energy bands near the band edge are mainly contributed by Pb and I atoms, while those contributed by the organic molecules are deep in

the energy level. After including the SOC, the electronic band undergoes splitting along the momentum ( $k$ ) directions in both the conduction band (CB) and the valence band (VB), with the more intense splitting in the CB usually ascribed to the presence of stronger SOC caused by Pb orbitals [103,108]. Such different degrees of Rashba-like band splitting in the band edges can give rise to the dual PL emission as observed in experiments, yet the origin of such splitting needs to be explored further. Note that the band splitting is anisotropic in the band structure, especially in the conduction band [Fig. 3(a)], which is further reflected in the calculated Rashba coefficients ( $\alpha_R = 2\Delta E_R/k_R$ ) [6,109] around the band edges [i.e., the high-symmetry point  $B$  in the Brillouin zone, Fig. 3(b)]. Here,  $\alpha_R$  has maximal values along the  $k_y$  direction and minimal values (almost zero) along the  $k_z$  direction in both CB and VB edges [Figs. 3(a) and 3(c)].

To understand the observed Rashba anisotropy, we then analyzed the Rashba splitting within the whole Brillouin zone. It is easy to find that the band splitting in the CB mainly occurs in the  $Y-A$  ( $k_x$ ) and  $B-A$  ( $k_y$ ) directions, while no splitting occurs in the  $G-Z$  ( $k_z$ ) or  $B-D$  ( $k_z$ ) direction [Fig. 3(a)]. This indicates that the Rashba band splitting in the CB basically takes place within the  $k_x-k_y$  plane. According to the traditional 2D Rashba model, the Rashba Hamiltonian is defined as [109]  $H_R^{2D} = \alpha_R^{2D} (\mathbf{k} \times \hat{z}) \cdot \sigma = \alpha_R^{2D} (k_y \sigma_x - k_x \sigma_y)$ , where  $\alpha_R^{2D}$  is the 2D Rashba coefficient,  $\sigma = (\sigma_x, \sigma_y, \sigma_z)$  is the Pauli matrix,  $\mathbf{k} = (k_x, k_y, k_z)$  is the wave vector, and  $\hat{z}$  is the surface normal representing the out-of-plane direction. From this model, the potential gradient in the  $z$  direction can induce an effective magnetic field in the orthogonal  $x-y$  (or  $k_x-k_y$ ) plane (also called the  $k$ -point sampling plane), which can interact with the electron spin and result in the Rashba spin splitting in that sampling plane. Based on this, the above calculations indicate that the energy band splitting of the CB in the  $k_x-k_y$  plane is most likely due to the existence of a potential gradient along the  $z$  direction, i.e., the presence of a structural symmetry breaking in the  $z$  direction. This is further verified by the calculations of the orbital contributions to the band splitting. The orbital projected band structure calculations show that the band splitting of the CB in the  $k_x-k_y$  plane is mainly contributed by the  $p_z$  orbital of Pb [Figs. 3(d) and 3(e)], implying that the symmetry breaking along the  $p_z$  orbital direction produces an effective Rashba field in the  $k_x-k_y$  ( $x-y$ ) plane and thus induces the band splitting of the CB in this plane. However, it is worth noting that the out-of-plane direction (i.e., the stacking direction) of (AMP)PbI<sub>4</sub> is along the  $x$  direction [i.e., the  $a$ -axis direction of the structure shown in Fig. 1(a)], and the  $y-z$  ( $b-c$ ) plane is indeed the 2D plane where the inorganic octahedra locate. This means that the band splitting of the CB in the  $k_x-k_y$  plane is in fact caused mainly by an in-plane potential gradient along the  $z$  ( $c$ -axis) direction for (AMP)PbI<sub>4</sub>, unlike in most reported materials where the (in-plane) Rashba splitting usually results from an out-of-plane potential gradient [6,23,25,110]. This somehow coincides with the structural deformation analysis, where substantial in-plane distortion was found in (AMP)PbI<sub>4</sub> due to the strong hydrogen bonding interaction with the organic cations (Note 4 in the Supplemental Material [97]). In addition, the AMP organic cations orient alternatively with an up-and-down configuration along the in-plane axes

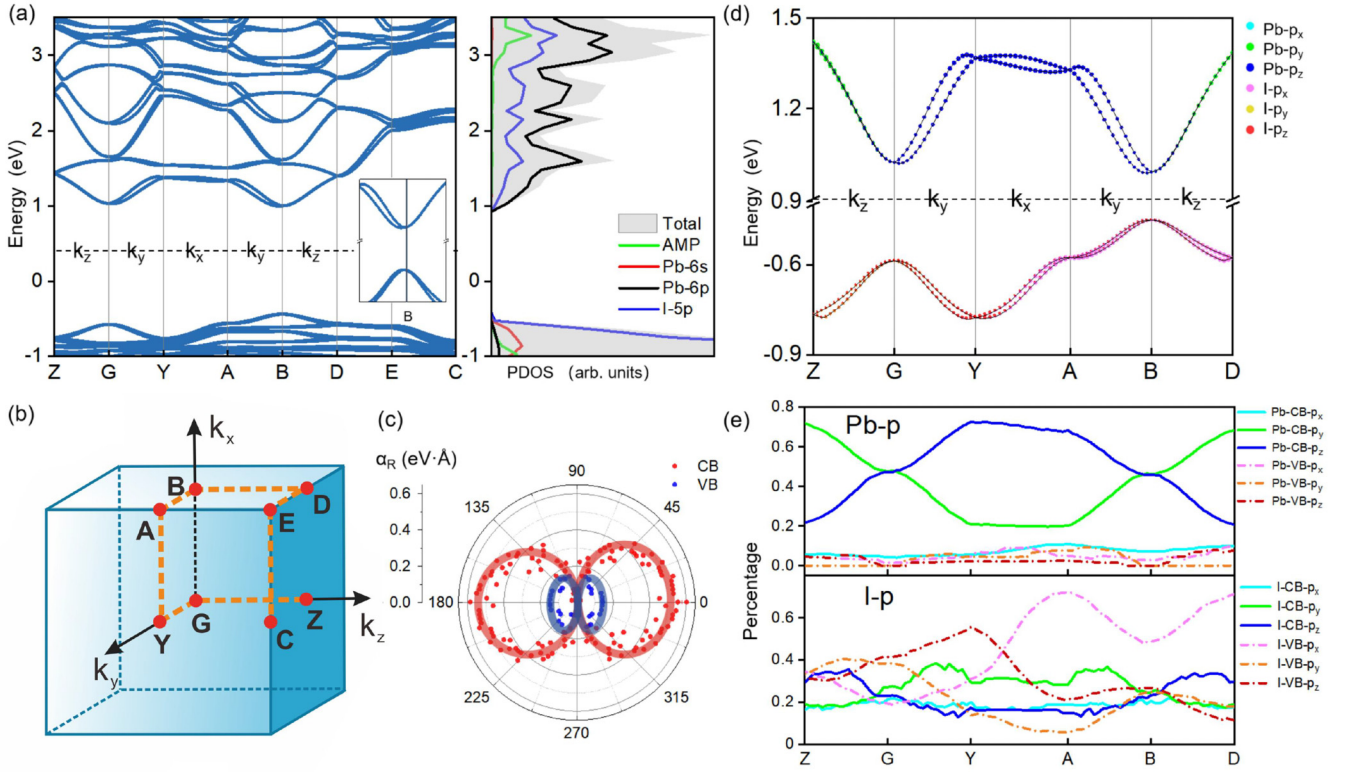


FIG. 3. (a) Electronic band structure (left) and projected density of states (right) of (AMP)PbI<sub>4</sub> calculated with spin-orbit coupling (SOC). Insets show the magnified splitting at the band gap extrema around the *B* point. (b) Brillouin zone with the high-symmetry points labeled by the capital letters. (c) Polar plots of  $\alpha_R$  in both the conduction band (CB) and valence band (VB) around the *B* point with the splitting along the  $k_y$ – $k_z$  in-plane directions. (d) Orbital projected band diagrams for (AMP)PbI<sub>4</sub>. (e) Percentages of Pb-*p* and I-*p* orbitals in both CB and VB.

[Fig. 1(a)] [80], further implying the in-plane asymmetry in the crystal structure. Such prominent in-plane distortion plus the in-plane structural asymmetry point to the sufficient in-plane potential gradient for the obvious out-of-plane splitting in the CB, like the cases rarely reported in some alloyed metal surfaces and layered materials [24,33,34,36,111,112]. However, for the case in the VB, the band splitting is much smaller and occurs along the three momentum directions [ $k_x$ ,  $k_y$ , and  $k_z$ , Fig. 3(a)]. The orbital projected band structure calculations show that the band splitting of the VB is mainly contributed by the  $p_z$  and  $p_x$  orbitals of I [Figs. 3(d) and 3(e)], meaning that both in-plane (along the  $z$  direction) and out-of-plane (along the  $x$  direction) potential gradients contribute to this splitting. The presence of out-of-plane potential gradient in (AMP)PbI<sub>4</sub> is predictable since its organic cation configuration can also break the out-of-plane symmetry and produce a permanent electric polarization along this direction, which was considered the origin of its robust ferroelectricity [80,83] and usually taken for granted as the cause of the observed Rashba effect in this perovskite. It is worth noting that, although the organic cations have no remarkable effect on the band edge, their interactions with the inorganic octahedra and their configuration in the perovskites can significantly modify the structure symmetry, thus contributing to both in-plane and out-of-plane symmetry breaking in the studied system. These all give rise to the observed 3D Rashba band splitting with the out-of-plane splitting in the CB being the strongest, which further validates the formation of a momentum-indirect band

in (AMP)PbI<sub>4</sub> and is indeed the origin of the band splitting observed in the experiments.

The presence of the out-of-plane splitting suggests that the traditional 2D Rashba model is no longer adequate to describe our results. Thereby, a 3D Rashba model was introduced to describe the observed phenomena. Based on the Hamiltonian of SOC [3,113]:

$$H_{\text{SOC}} = \frac{e\hbar}{4m_0^2 c^2} [\nabla V \times \mathbf{P}] \cdot \sigma, \quad (1)$$

where  $e$  ( $m_0$ ) is the electron charge (mass),  $\hbar$  is the reduced Planck's constant,  $c$  is the velocity of light, and  $\nabla V$  ( $\mathbf{P}$ ) is the 3D potential gradient (momentum operator), the 3D Rashba Hamiltonian can be described as

$$\begin{aligned} H_{\text{R}}^{3\text{D}} &= \frac{\alpha_0 e\hbar}{4m_0^2 c^2} [\nabla V \times \mathbf{P}] \cdot \sigma = \frac{\alpha_0 e\hbar}{4m_0^2 c^2} [\mathbf{P} \times \mathbf{E}] \cdot \sigma \\ &= \frac{\alpha_0 e\hbar^2}{4m_0^2 c^2} [\mathbf{k} \times \mathbf{E}] \cdot \sigma, \end{aligned} \quad (2)$$

where  $\alpha_0$  is the Rashba primary correlation factor [107,109,114,115],  $\mathbf{E} = (E_x, E_y, E_z) = -\nabla V$  is the 3D electric field, and the relationship  $\mathbf{P} = \hbar\mathbf{k}$  is used. By applying the vector operation rules, the above 3D Rashba



Hamiltonian can be further spread as

$$\begin{aligned}
 H_{\text{R}}^{3\text{D}} &= \underbrace{\frac{\alpha_0 e \hbar^2}{4m_0^2 c^2} \begin{cases} [E_x(k_z \sigma_y - k_y \sigma_z) \\ + E_y(k_x \sigma_z - k_z \sigma_x) \\ + E_z(k_y \sigma_x - k_x \sigma_y)] \end{cases}}_{(3)} \\
 &= \underbrace{\begin{cases} \alpha_{\text{R}}(E_x)(k_z \sigma_y - k_y \sigma_z) \\ + \alpha_{\text{R}}(E_y)(k_x \sigma_z - k_z \sigma_x) \\ + \alpha_{\text{R}}(E_z)(k_y \sigma_x - k_x \sigma_y) \end{cases}}_{(4)} \\
 &= \underbrace{\begin{cases} k_x [\alpha_{\text{R}}(E_y) \sigma_z - \alpha_{\text{R}}(E_z) \sigma_y] \\ + k_y [\alpha_{\text{R}}(E_z) \sigma_x - \alpha_{\text{R}}(E_x) \sigma_z] \\ + k_z [\alpha_{\text{R}}(E_x) \sigma_y - \alpha_{\text{R}}(E_y) \sigma_x] \end{cases}}_{(5)} \\
 &= \underbrace{\begin{cases} \frac{2}{\hbar} S_x [\alpha_{\text{R}}(E_z) k_y - \alpha_{\text{R}}(E_y) k_z] \\ + \frac{2}{\hbar} S_y [\alpha_{\text{R}}(E_x) k_z - \alpha_{\text{R}}(E_z) k_x] \\ + \frac{2}{\hbar} S_z [\alpha_{\text{R}}(E_y) k_x - \alpha_{\text{R}}(E_x) k_y] \end{cases}}_{(6)},
 \end{aligned}$$

where  $\alpha_{\text{R}}(E_i) = \frac{\alpha_0 e \hbar^2}{4m_0^2 c^2} E_i$  ( $i = x, y,$  and  $z$ ) is defined as the 3D Rashba coefficient and is a function of the electric field, and  $\mathbf{S} = (S_x, S_y, S_z) = \frac{\hbar}{2}(\sigma_x, \sigma_y, \sigma_z)$  is the spin operator. According to this model, if there is a Rashba splitting along the  $k_x$  direction, then either  $\alpha_{\text{R}}(E_z)$  or  $\alpha_{\text{R}}(E_y)$  or both should have nonzero values [see Eq. (5) in the 3D Rashba Hamiltonian], meaning that there exists a potential gradient either in the  $z$  or  $y$  direction or both. As a result, the split bands along the  $k_x$  direction should have orbital contributions from either the  $p_z$  or  $p_y$  orbital or both (assuming that the bands are mainly contributed by  $p$  orbitals and no external electric field is applied, just like the case here). Likewise, if the Rashba splitting occurs along the  $k_y$  ( $k_z$ ) direction, then the split bands in that direction should at least have orbital contributions from one of the  $p_z$  or  $p_x$  ( $p_x$  or  $p_y$ ) orbitals. This phenomenological model is very consistent with the calculations of the orbital projected band structure and the related orbital proportions for (AMP)PbI<sub>4</sub> [Figs. 3(d) and 3(e)]. In addition, the Rashba anisotropy can be explained in terms of this 3D model. Since the splitting occurs within the 3D space, then different potential gradients in each direction can produce different degrees of splitting, leading to the observed anisotropic splitting.

Moreover, the spin-polarization analysis and calculations carried out below further validate the presence of 3D Rashba spin splitting in (AMP)PbI<sub>4</sub>, with the out-of-plane spin polarization being dominant in the overall splitting. Based on the above 3D Rashba model, there should exist spin polarization along the three momentum directions, and the momentum distributions of the expectation values of the spin operator [ $\langle \mathbf{S} \rangle = (\langle S_x \rangle, \langle S_y \rangle, \langle S_z \rangle)$ ] can be predicted from this model. For instance, if there exists spin polarization along the  $x$  direction, then nonzero  $\langle S_x \rangle$  should be observed in the band structure along either the  $k_y$  or  $k_z$  direction or both, accompanied by the existence of a potential gradient either in the  $z$  or  $y$  direction or both [see Eq. (6) in the 3D Rashba Hamiltonian].

This is very consistent with the calculation results of the band structures with projected spin expectation values [Figs. 4(a)–4(c)]. As seen, nonzero  $\langle S_x \rangle$  was indeed observed along the  $k_y$  direction in both the CB and VB [Fig. 4(a)], meaning that a potential gradient along the  $z$  direction or an in-plane symmetry breaking exists in the system to split the bands in both the CB and VB [note that the out-of-plane direction for (AMP)PbI<sub>4</sub> is the  $x$  direction]. The mutually perpendicular spin ( $S_x$ ) and momentum ( $k_y$ ) directions indicate that this spin splitting is indeed Rashba type. Similarly, if the spin polarizes along the  $y$  ( $z$ ) direction, then nonzero  $\langle S_y \rangle$  ( $\langle S_z \rangle$ ) should be observed in the band structure at least in one of the  $k_z$  or  $k_x$  ( $k_x$  or  $k_y$ ) directions, along with a potential gradient existing in at least one of the  $x$  or  $z$  ( $y$  or  $x$ ) directions [Eq. (6)]. As expected, nonzero  $\langle S_y \rangle$  was in fact observed in the CB mainly along the  $k_x$  direction [Fig. 4(b)], further suggesting that the potential gradient along the  $z$  direction or the in-plane symmetry breaking mainly contributes to the splitting in the CB. Meanwhile, nonzero  $\langle S_y \rangle$  was also observed in the VB along both  $k_z$  and  $k_x$  directions [Fig. 4(b)], indicating that both out-of-plane symmetry breaking (with a potential gradient in the  $x$  direction) and in-plane symmetry breaking (with a potential gradient in the  $z$  direction) take place in the system to cause the spin splitting in the VB. Finally, for the spin polarization  $S_z$ , nonzero  $\langle S_z \rangle$  was found in the VB along the  $k_y$  direction [Fig. 4(c)], suggesting a potential gradient existing in the  $x$  direction and thus an out-of-plane symmetry breaking contributing to this splitting in the VB. These results not only verify the rationality of the 3D Rashba model but also support the fact that the spin splitting in the CB is mainly caused by the in-plane symmetry breaking, while that in the VB is contributed by both in-plane and out-of-plane symmetry breaking, with the spin splitting along the out-of-plane direction ( $\langle S_x \rangle$ ) being the most significant [Figs. 4(a)–4(c)]. It is worth mentioning that the above discussion involves the band spin splitting and related spin polarization within the whole Brillouin zone, and thus, the 3D Rashba model must be applied to interpret all the spin-polarization behaviors in this region. For the spin splitting at a specific high-symmetry point such as the  $B$  point in the Brillouin zone, the effective Hamiltonian converges to the 2D model with its potential gradient direction either along the in-plane or out-of-plane direction, depending on the polarization direction of the crystal structure as well as the orbital contributions to the energy bands at this specific point (see Note 5 in the Supplemental Material [97] for detail). Finally, the spin contours around the band edges ( $B$  point) at constant energies of 1.2 eV in the CB and  $-0.5$  eV in the VB were calculated to further confirm the origin of the spin splitting in (AMP)PbI<sub>4</sub> [Figs. 4(d)–4(i)]. As seen, the sign of the spin polarization in  $x, y,$  and  $z$  direction ( $S_x, S_y, S_z$ ) was found to be opposite when projected along a momentum direction that is perpendicular to it, which is another hallmark of the Rashba spin splitting in the studied system.

Note that the above DFT calculations were carried out at 0 K, which principally elucidate the static Rashba effect involved in the studied system, whereas experiments are usually carried out at much higher temperatures, and thermal distortion could also induce Rashba splitting, called the dynamical Rashba effect, in the perovskites as previously reported [64,87,101,107]; therefore, AIMD simulations were

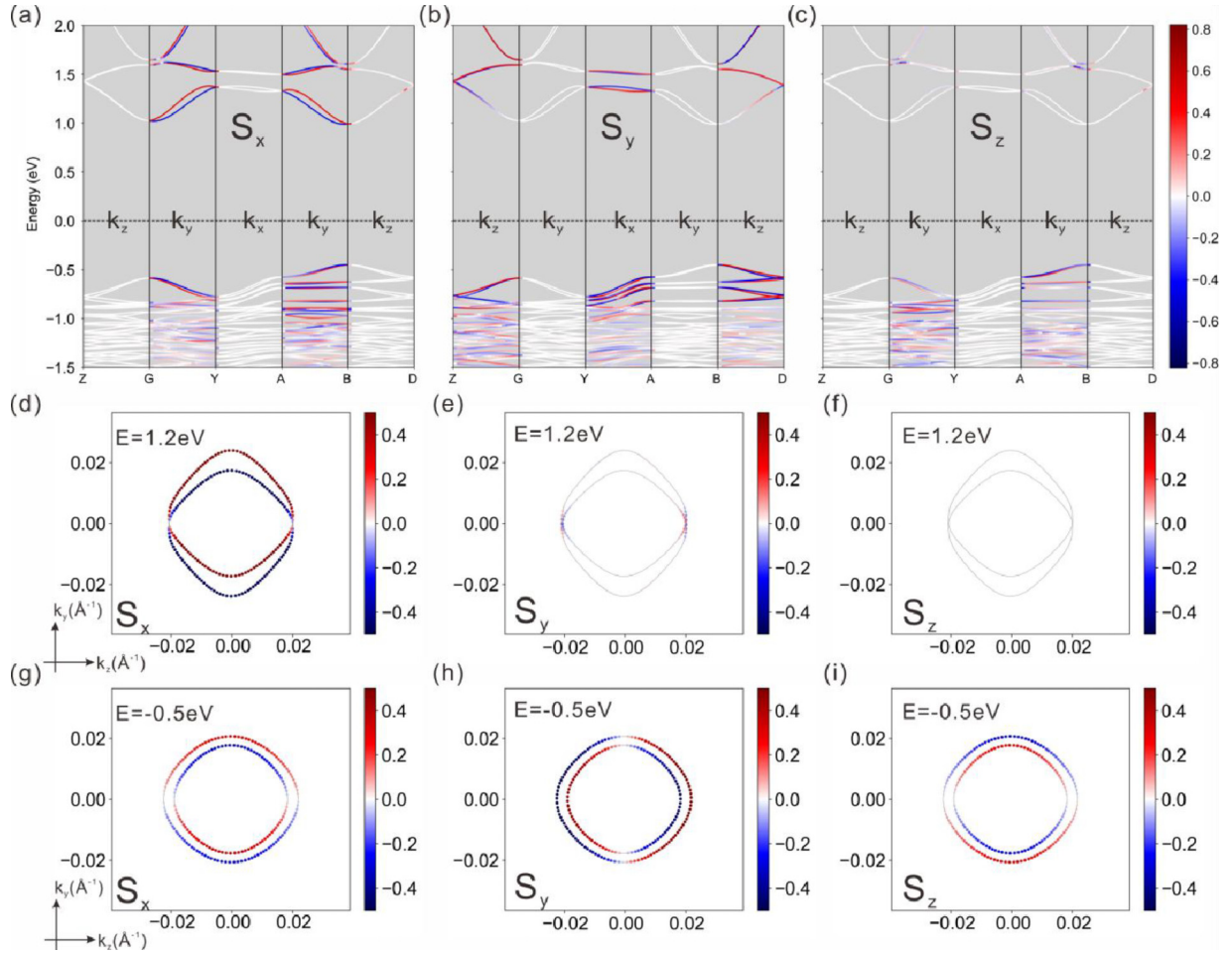


FIG. 4. (a)–(c) Calculated band structures with projected expectation values of the spin operator on the spinor wave functions ( $\langle S_x \rangle$ ,  $\langle S_y \rangle$ ,  $\langle S_z \rangle$ ) for (AMP)PbI<sub>4</sub>. Calculated spin contours in  $x$ ,  $y$ , and  $z$  directions around the  $B$  point at the constant energies of (d)–(f) 1.2 eV in the conduction band (CB) and (g)–(i)  $-0.5$  eV in the valence band (VB). The scale bars shown on the right represent the intensity scales.

performed further for (AMP)PbI<sub>4</sub> to account for this temperature effect. The crystal structures of (AMP)PbI<sub>4</sub> at 80, 250, and 300 K were first simulated as shown in Figs. 5(a)–5(c). Obviously, the structure distortion is strengthened when increasing the temperature  $>0$  K. Correspondingly, the degree of Rashba spin splitting becomes much more significant across the whole Brillouin zone [Figs. 5(d)–5(f)], indicating the presence of the dynamical Rashba effect. Additionally, the orbital projected band structure calculations demonstrate that the notable band splitting in the CB and VB is mainly contributed by the  $p$  (including  $p_z$ ,  $p_y$ , and  $p_x$ ) orbitals of Pb and I [Figs. 5(d)–5(f)], indicating that both in-plane and out-of-plane symmetry breaking is responsible for the splitting in the band edges. However, the out-of-plane spin splitting in the CB owing to the in-plane symmetry breaking of the crystal field always dominates the overall splitting for all the simulated temperatures [Figs. 5(d)–5(f)], just like the case at 0 K. This was further verified by the spin-polarization calculations, where the out-of-plane spin polarization ( $S_x$ ) is always the dominant component at all simulated temperatures (Figs. S6(a)–S6(c), S7(a)–S7(c), and S8(a)–S8(c) in the Supplemental Material [97]). In addition, the fixed-energy spin contours around the band edges ( $B$  point) were calculated to confirm the

nature of the spin splitting being Rashba type in (AMP)PbI<sub>4</sub> (Figs. 5(g)–5(i), S6(d)–S6(i), S7(d)–S7(i), and S8(d)–S8(i) in the Supplemental Material [97]). Note that there exist uncertainties to acquire the accurate trend of the Rashba splitting varying with the temperature since the calculated band structures based on AIMD simulations are instantaneous ones due to the continuous atomic vibrations. Nonetheless, these results suggest that both static and dynamic Rashba effects contribute to the overall Rashba spin splitting, with the out-of-plane spin polarization always prevailing in the studied DJ perovskite.

#### IV. CONCLUSIONS

In conclusion, we found that the large Rashba spin splitting in the layered DJ perovskite (AMP)PbI<sub>4</sub> was contributed mainly by the out-of-plane spin polarization, manifesting the strong in-plane symmetry breaking of the crystal field in the studied system. Additionally, the interpretation of the overall Rashba spin splitting in the system requires a 3D Rashba model, which features the classic spin-momentum locking property and possesses a dominant out-of-plane spin component plus two relatively weaker in-plane ones in the band structures. Moreover, the temperature-dependent Rashba



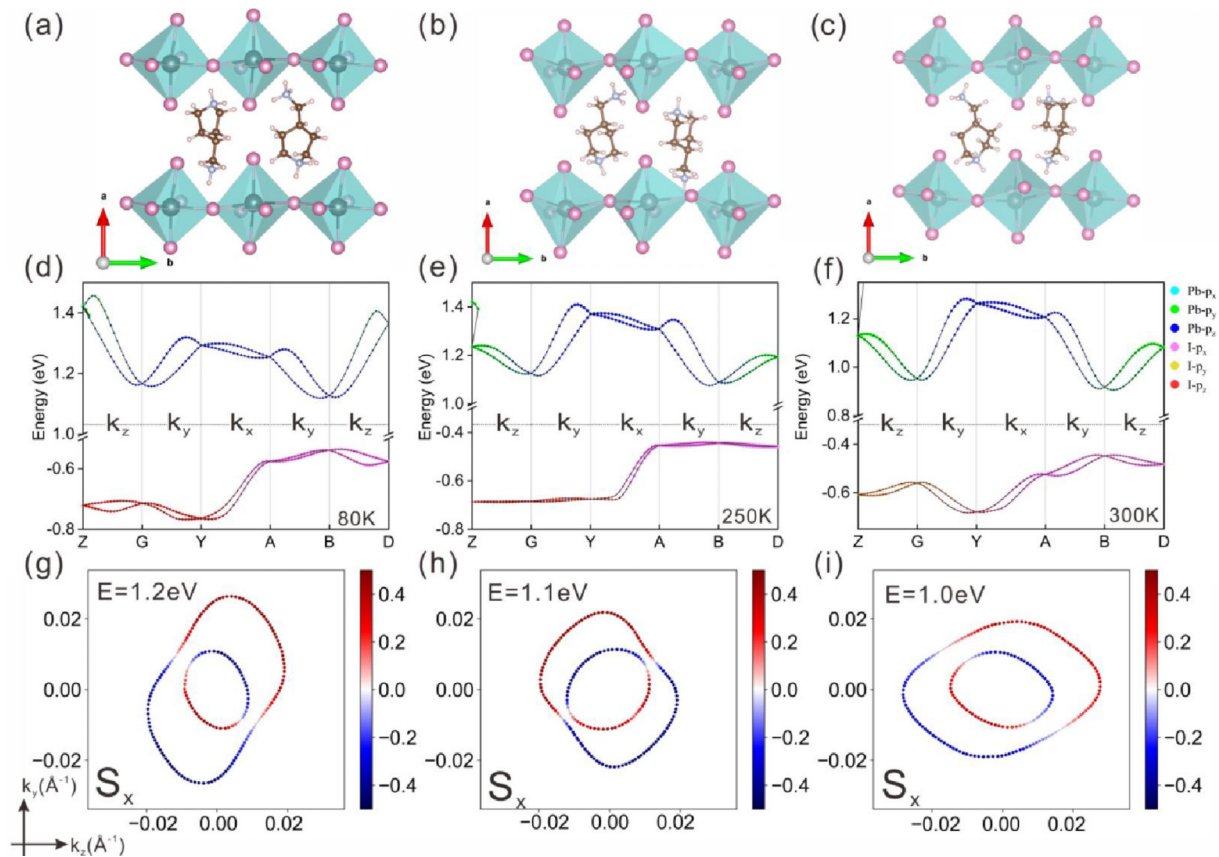


FIG. 5. Crystal structures of (AMP)PbI<sub>4</sub> at (a) 80 K, (b) 250 K, and (c) 300 K. *a*, *b*, and *c* denote the crystal axis directions. Orbital projected band structures of (AMP)PbI<sub>4</sub> at (d) 80 K, (e) 250 K, and (f) 300 K. Calculated spin contours in the *x* direction around the *B* point at the constant energy of (g) 1.2 eV under 80 K, (h) 1.1 eV under 250 K, and (i) 1.0 eV under 300 K. The scale bars shown on the right represent the intensity scales.

spin splitting shows that the total spin splitting arises from both static and dynamical Rashba effects, with the out-of-plane spin polarization always surpassing the in-plane ones for the spin splitting. This indicates that the in-plane structure distortion by lattice vibrations in this system is mainly responsible for the out-of-plane spin splitting, rather than the commonly considered in-plane spin splitting. Our results demonstrate that the studied DJ perovskite is a good archetype for exploring the out-of-plane spin polarization, which is a very attractive property for developing field-free high-density memories. Meanwhile, the large Rashba spin splitting in the DJ perovskite makes the Rashba SOC directly accessible by spectroscopic techniques. Integrating the other advantages like flexibly tunable SOC via structural and chemical engineering, excellent ambient stability, and low-cost preparation, the DJ perovskite may serve as a powerful platform for manipulating the spin texture for the desired spintronics. Moreover, the presence of out-of-plane spin polarization along with the previously reported ferroelectricity makes DJ

perovskites even more promising in the field of spin-based logic in-memory computing.

#### ACKNOWLEDGMENTS

We thank Zheyuan Xu, Boyi Xu, Jinyue Fu, Xiaoli Zhu, and Xianwei Fu for stimulating discussions. We are also grateful to the National Natural Science Foundation of China (Grants No. 52072117, No. 51972105, No. 11704111, No. 52221001, No. 62090035, and No. U19A2090), the Hunan Provincial Natural Science Foundation of China (Grant No. 2021JJ30132), the National Key R&D Program of China (Grant No. 2022YFA1204300) and the Key Program of Science and Technology Department of Hunan Province (Grants No. 2019XK2001 and No. 2020XK2001). We are grateful for the computing resources provided by the National Supercomputing Center in Shenzhen (Shenzhen Cloud Computing Center).

R.X. and P.C. contributed equally to this paper.

[1] F. Trier, P. Noël, J. Kim, J. Attané, L. Vila, and M. Bibes, Oxide spin-orbitronics: Spin-charge interconversion and topological spin textures, *Nat. Rev. Mater.* **7**, 258 (2022).

[2] G. Bihlmayer, P. Noël, D. V. Vyalikh, E. V. Chulkov, and A. Manchon, Rashba-like physics in condensed matter, *Nat. Rev. Phys.* **4**, 642 (2022).

- [3] A. Manchon, Rashba spin orbit coupling in two-dimensional systems, in *Spintronic 2D Materials* (Elsevier, Netherlands, 2020).
- [4] A. Manchon, H. C. Koo, J. Nitta, S. M. Frolov, and R. A. Duine, New perspectives for Rashba spin-orbit coupling, *Nat. Mater.* **14**, 871 (2015).
- [5] C. Song, R. Zhang, L. Liao, Y. Zhou, X. Zhou, R. Chen, Y. You, X. Chen, and F. Pan, Spin-orbit torques: Materials, mechanisms, performances, and potential applications, *Prog. Mater. Sci.* **118**, 100761 (2021).
- [6] J. Chen, K. Wu, W. Hu, and J. Yang, Spin-orbit coupling in 2D semiconductors: A theoretical perspective, *J. Phys. Chem. Lett.* **12**, 12256 (2021).
- [7] V. M. Edelstein, Spin polarization of conduction electrons induced by electric current in two-dimensional asymmetric electron systems, *Solid State Commun.* **73**, 233 (1990).
- [8] H. Isshiki, P. Muduli, J. Kim, K. Kondou, and Y. Otani, Phenomenological model for the direct and inverse Edelstein effects, *Phys. Rev. B* **102**, 184411 (2020).
- [9] Y. K. Kato, R. C. Myers, A. C. Gossard, and D. D. Awschalom, Current-Induced Spin Polarization in Strained Semiconductors, *Phys. Rev. Lett.* **93**, 176601 (2004).
- [10] K. E. Strecker, G. B. Partridge, A. G. Truscott, and R. G. Hulet, Formation and propagation of matter-wave soliton trains, *Nature (London)* **417**, 150 (2002).
- [11] H. An, T. Ohno, Y. Kanno, Y. Kageyama, Y. Monnai, H. Maki, J. Shi, and K. Ando, Current-induced magnetization switching using anelectrically insulating spin-torque generator, *Sci. Adv.* **4**, eaar2250 (2018).
- [12] J. Han, A. Richardella, S. Siddiqui, J. Finley, N. Samarth, and L. Liu, Room-Temperature Spin-Orbit Torque Switching Induced by a Topological Insulator, *Phys. Rev. Lett.* **119**, 077702 (2017).
- [13] Y. Fan, P. Upadhyaya, X. Kou, M. Lang, S. Takei, Z. Wang, J. Tang, L. He, L. T. Chang, M. Montazeri *et al.*, Magnetization switching through giant spin-orbit torque in a magnetically doped topological insulator heterostructure, *Nat. Mater.* **13**, 699 (2014).
- [14] S. Datta and B. Das, Electronic analog of the electro-optic modulator, *Appl. Phys. Lett.* **56**, 665 (1990).
- [15] H. C. Koo, J. H. Kwon, J. Eom, J. Chang, S. H. Han, and M. Johnson, Control of spin precession in a spin-injected field effect transistor, *Science* **325**, 1515 (2009).
- [16] P. Chuang, S. Ho, L. W. Smith, F. Sfigakis, M. Pepper, C. Chen, J. Fan, J. P. Griffiths, I. Farrer, H. E. Beere *et al.*, All-electric all-semiconductor spin field-effect transistors, *Nat. Nanotechnol.* **10**, 35 (2015).
- [17] S. Datta, How we proposed the spin transistor, *Nat. Electron.* **1**, 604 (2018).
- [18] X. Qiu, K. Narayanapillai, Y. Wu, P. Deorani, D.-H. Yang, W.-S. Noh, J.-H. Park, K.-J. Lee, H.-W. Lee, and H. Yang, Spin-orbit-torque engineering via oxygen manipulation, *Nat. Nanotechnol.* **10**, 333 (2015).
- [19] S. Manipatruni, D. E. Nikonov, C. C. Lin, T. A. Gosavi, H. Liu, B. Prasad, Y. L. Huang, E. Bonturim, R. Ramesh, and I. A. Young, Scalable energy-efficient magnetoelectric spin-orbit logic, *Nature (London)* **565**, 35 (2019).
- [20] T. Seifert, S. Jaiswal, U. Martens, J. Hannegan, L. Braun, P. Maldonado, F. Freimuth, A. Kronenberg, J. Henrizi, I. Radu *et al.*, Efficient metallic spintronic emitters of ultrabroadband terahertz radiation, *Nat. photonics* **10**, 483 (2016).
- [21] L. Cheng, Z. Li, D. Zhao, and E. E. M. Chia, Studying spin-charge conversion using terahertz pulses, *APL Mater.* **9**, 070902 (2021).
- [22] A. Soumyanarayanan, N. Reyren, A. Fert, and C. Panagopoulos, Emergent phenomena induced by spin-orbit coupling at surfaces and interfaces, *Nature (London)* **539**, 509 (2016).
- [23] J. Nitta, T. Akazaki, and H. Takayanagi, Gate Control of Spin-Orbit Interaction in an Inverted  $\text{In}_{0.53}\text{Ga}_{0.47}\text{As}/\text{In}_{0.52}\text{Al}_{0.48}\text{As}$  Heterostructure, *Phys. Rev. Lett.* **78**, 1335 (1997).
- [24] C. R. Ast, J. Henk, A. Ernst, L. Moreschini, M. C. Falub, D. Pacile, P. Bruno, K. Kern, and M. Grioni, Giant Spin Splitting Through Surface Alloying, *Phys. Rev. Lett.* **98**, 186807 (2007).
- [25] G. Bihlmayer, Y. M. Koroteev, P. M. Echenique, E. V. Chulkov, and S. Blügel, The Rashba-effect at metallic surfaces, *Surf. Sci.* **600**, 3888 (2006).
- [26] M. Chen and F. Liu, Prediction of giant and ideal Rashba-type splitting in ordered alloy monolayers grown on a polar surface, *Natl. Sci. Rev.* **8**, nwa241 (2021).
- [27] D. Di Sante, P. Barone, R. Bertacco, and S. Picozzi, Electric control of the giant Rashba effect in bulk GeTe, *Adv. Mater.* **25**, 509 (2013).
- [28] S. Gupta and B. I. Yakobson, What dictates Rashba splitting in 2D van der Waals heterobilayers, *J. Am. Chem. Soc.* **143**, 3503 (2021).
- [29] K. Ishizaka, M. S. Bahramy, H. Murakawa, M. Sakano, T. Shimojima, T. Sonobe, K. Koizumi, S. Shin, H. Miyahara, A. Kimura *et al.*, Giant Rashba-type spin splitting in bulk BiTeI, *Nat. Mater.* **10**, 521 (2011).
- [30] P. D. King, R. C. Hatch, M. Bianchi, R. Ovsyannikov, C. Lupulescu, G. Landolt, B. Slomski, J. H. Dil, D. Guan, J. L. Mi *et al.*, Large Tunable Rashba Spin Splitting of a Two-Dimensional Electron Gas in  $\text{Bi}_2\text{Se}_3$ , *Phys. Rev. Lett.* **107**, 096802 (2011).
- [31] A. Varykhalov, D. Marchenko, M. R. Scholz, E. D. Rienks, T. K. Kim, G. Bihlmayer, J. Sanchez-Barriga, and O. Rader, Ir(111) Surface State with Giant Rashba Splitting Persists Under Graphene in Air, *Phys. Rev. Lett.* **108**, 066804 (2012).
- [32] Q.-F. Yao, J. Cai, W.-Y. Tong, S.-J. Gong, J.-Q. Wang, X. Wan, C.-G. Duan, and J. H. Chu, Manipulation of the large Rashba spin splitting in polar two-dimensional transition-metal dichalcogenides, *Phys. Rev. B* **95**, 165401 (2017).
- [33] Y. Feng, Q. Jiang, B. Feng, M. Yang, T. Xu, W. Liu, X. Yang, M. Arita, E. F. Schwier, K. Shimada *et al.*, Rashba-like spin splitting along three momentum directions in trigonal layered  $\text{PtBi}_2$ , *Nat. Commun.* **10**, 4765 (2019).
- [34] R. Friedrich, V. Caciuc, G. Bihlmayer, N. Atodiresei, and S. Blügel, Designing the Rashba spin texture by adsorption of inorganic molecules, *New J. Phys.* **19**, 043017 (2017).
- [35] P. He, S. M. Walker, S. S. Zhang, F. Y. Bruno, M. S. Bahramy, J. M. Lee, R. Ramaswamy, K. Cai, O. Heinonen, G. Vignale *et al.*, Observation of Out-of-Plane Spin Texture in a  $\text{SrTiO}_3(111)$  Two-Dimensional Electron Gas, *Phys. Rev. Lett.* **120**, 266802 (2018).
- [36] S.-H. Zhang and B.-G. Liu, Anisotropic Rashba effect and charge and spin currents in monolayer BiTeI by controlling symmetry, *Phys. Rev. B* **100**, 165429 (2019).

- [37] L. Liu, C.-F. Pai, Y. Li, H. W. Tseng, D. C. Ralph, and R. A. Buhrman, Spin-torque switching with the giant spin Hall effect of tantalum, *Science* **336**, 555 (2012).
- [38] G. Yu, P. Upadhyaya, Y. Fan, J. G. Alzate, W. Jiang, K. L. Wong, S. Takei, S. A. Bender, M. Lang, J. Tang *et al.*, Switching of perpendicular magnetization by spin-orbit torques in the absence of external magnetic fields, *Nat. Nanotechnol.* **9**, 548 (2014).
- [39] S. C. Baek, V. P. Amin, Y. W. Oh, G. Go, S. J. Lee, G. H. Lee, K. J. Kim, M. D. Stiles, B. G. Park, and K. J. Lee, Spin currents and spin-orbit torques in ferromagnetic trilayers, *Nat. Mater.* **17**, 509 (2018).
- [40] K. Cai, M. Yang, H. Ju, S. Wang, Y. Ji, B. Li, K. W. Edmonds, Y. Sheng, B. Zhang, N. Zhang *et al.*, Electric field control of deterministic current-induced magnetization switching in a hybrid ferromagnetic/ferroelectric structure, *Nat. Mater.* **16**, 712 (2017).
- [41] X. Chen, S. Shi, G. Shi, X. Fan, C. Song, X. Zhou, H. Bai, L. Liao, Y. Zhou, H. Zhang *et al.*, Observation of the antiferromagnetic spin Hall effect, *Nat. Mater.* **20**, 800 (2021).
- [42] S. Fukami, C. Zhang, S. DuttaGupta, A. Kurenkov, and H. Ohno, Magnetization switching by spin-orbit torque in an antiferromagnet-ferromagnet bilayer system, *Nat. Mater.* **15**, 535 (2016).
- [43] Y. Hibino, K. Hasegawa, T. Koyama, and D. Chiba, Spin-orbit torque generated by spin-orbit precession effect in Py/Pt/Co tri-layer structure, *APL Mater.* **8**, 041110 (2020).
- [44] Y. Hibino, T. Taniguchi, K. Yakushiji, A. Fukushima, H. Kubota, and S. Yuasa, Giant charge-to-spin conversion in ferromagnet via spin-orbit coupling, *Nat. Commun.* **12**, 6254 (2021).
- [45] A. M. Humphries, T. Wang, E. R. J. Edwards, S. R. Allen, J. M. Shaw, H. T. Nembach, J. Q. Xiao, T. J. Silva, and X. Fan, Observation of spin-orbit effects with spin rotation symmetry, *Nat. Commun.* **8**, 911 (2017).
- [46] M. Kimata, H. Chen, K. Kondou, S. Sugimoto, P. K. Muduli, M. Ikhlas, Y. Omori, T. Tomita, A. H. MacDonald, S. Nakatsuji *et al.*, Magnetic and magnetic inverse spin Hall effects in a non-collinear antiferromagnet, *Nature (London)* **565**, 627 (2019).
- [47] Y. C. Lau, D. Betto, K. Rode, J. M. Coey, and P. Stamenov, Spin-orbit torque switching without an external field using interlayer exchange coupling, *Nat. Nanotechnol.* **11**, 758 (2016).
- [48] Q. Ma, Y. Li, D. B. Gopman, Y. P. Kabanov, R. D. Shull, and C. L. Chien, Switching a Perpendicular Ferromagnetic Layer by Competing Spin Currents, *Phys. Rev. Lett.* **120**, 117703 (2018).
- [49] D. MacNeill, G. M. Stiehl, M. H. D. Guimaraes, R. A. Buhrman, J. Park, and D. C. Ralph, Control of spin-orbit torques through crystal symmetry in WTe<sub>2</sub>/ferromagnet bilayers, *Nat. Phys.* **13**, 300 (2016).
- [50] I. M. Miron, K. Garello, G. Gaudin, P. J. Zermatten, M. V. Costache, S. Auffret, S. Bandiera, B. Rodmacq, A. Schuhl, and P. Gambardella, Perpendicular switching of a single ferromagnetic layer induced by in-plane current injection, *Nature (London)* **476**, 189 (2011).
- [51] T. Nan, C. X. Quintela, J. Irwin, G. Gurung, D. F. Shao, J. Gibbons, N. Campbell, K. Song, S. Choi, L. Guo *et al.*, Controlling spin current polarization through non-collinear antiferromagnetism, *Nat. Commun.* **11**, 4671 (2020).
- [52] Y. W. Oh, S. H. C. Baek, Y. M. Kim, H. Y. Lee, K. D. Lee, C. G. Yang, E. S. Park, K. S. Lee, K. W. Kim *et al.*, Field-free switching of perpendicular magnetization through spin-orbit torque in antiferromagnet/ferromagnet/oxide structures, *Nat. Nanotechnol.* **11**, 878 (2016).
- [53] Y. W. Oh, J. Ryu, J. Kang, and B. G. Park, Material and thickness investigation in ferromagnet/Ta/CoFeB trilayers for enhancement of spin-orbit torque and field-free switching, *Adv. Electron. Mater.* **5**, 1900598 (2019).
- [54] A. van den Brink, G. Vermijs, A. Solignac, J. Koo, J. T. Kohlhepp, H. J. M. Swagten, and B. Koopmans, Field-free magnetization reversal by spin-Hall effect and exchange bias, *Nat. Commun.* **7**, 10854 (2016).
- [55] T. Yokouchi and Y. Shiomi, Enhancement of Current-Induced Out-of-Plane Spin Polarization by Heavy-Metal-Impurity Doping in Fe Thin Films, *Phys. Rev. Appl.* **16**, 054001 (2021).
- [56] Y. You, H. Bai, X. Feng, X. Fan, L. Han, X. Zhou, Y. Zhou, R. Zhang, T. Chen, F. Pan *et al.*, Cluster magnetic octupole induced out-of-plane spin polarization in antiperovskite antiferromagnet, *Nat. Commun.* **12**, 6524 (2021).
- [57] A. L. Sharpe, E. J. Fox, A. W. Barnard, J. Finney, K. Watanabe, T. Taniguchi, M. A. Kastner, and D. Goldhaber-Gordon, Emergent ferromagnetism near three-quarters filling in twisted bilayer graphene, *Science* **365**, 605 (2019).
- [58] M. Serlin, C. L. Tschirhart, H. Polshyn, Y. Zhang, J. Zhu, K. Watanabe, T. Taniguchi, L. Balents, and A. F. Young, Intrinsic quantized anomalous Hall effect in a moiré heterostructure, *Science* **367**, 900 (2020).
- [59] D. Niesner, M. Wilhelm, I. Levchuk, A. Osvet, S. Shrestha, M. Batentschuk, C. Brabec, and T. Fauster, Giant Rashba Splitting in CH<sub>3</sub>NH<sub>3</sub>PbBr<sub>3</sub> Organic-Inorganic Perovskite, *Phys. Rev. Lett.* **117**, 126401 (2016).
- [60] S. A. Bourelle, F. V. A. Camargo, S. Ghosh, T. Neumann, T. W. J. van de Goor, R. Shivanna, T. Winkler, G. Cerullo, and F. Deschler, Optical control of exciton spin dynamics in layered metal halide perovskites via polaronic state formation, *Nat. Commun.* **13**, 3320 (2022).
- [61] D. Giovanni, H. Ma, J. Chua, M. Gratzel, R. Ramesh, S. Mhaisalkar, N. Mathews, and T. C. Sum, Highly spin-polarized carrier dynamics and ultralarge photoinduced magnetization in CH<sub>3</sub>NH<sub>3</sub>PbI<sub>3</sub> perovskite thin films, *Nano Lett.* **15**, 1553 (2015).
- [62] E. Lafalce, E. Amerling, Z. G. Yu, P. C. Sercel, L. Whittaker-Brooks, and Z. V. Vardeny, Rashba splitting in organic-inorganic lead-halide perovskites revealed through two-photon absorption spectroscopy, *Nat. Commun.* **13**, 483 (2022).
- [63] P. Odenthal, W. Talmadge, N. Gundlach, R. Wang, C. Zhang, D. Sun, Z.-G. Yu, Z. V. Vardeny, and Y. S. Li, Spin-polarized exciton quantum beating in hybrid organic-inorganic perovskites, *Nat. Phys.* **13**, 894 (2017).
- [64] J. A. Steele, P. Puech, B. Monserrat, B. Wu, R. X. Yang, T. Kirchartz, H. Yuan, G. Fleury, D. Giovanni, E. Fron *et al.*, Role of electron-phonon coupling in the thermal evolution of bulk Rashba-like spin-split lead halide perovskites exhibiting dual-band photoluminescence, *ACS Energy Lett.* **4**, 2205 (2019).
- [65] M. Wang, H. Xu, T. Wu, H. Ambaye, J. Qin, J. Keum, I. N. Ivanov, V. Lauter, and B. Hu, Optically induced static magnetization in metal halide perovskite for spin-related optoelectronics, *Adv. Sci.* **8**, 2004488 (2021).



- [66] S. Yang, E. Vetter, T. Wang, A. Amassian, and D. Sun, Observation of long spin lifetime in MAPbBr<sub>3</sub> single crystals at room temperature, *J. Phys.: Mater.* **3**, 015012 (2020).
- [67] M. Zhou, J. S. Sarmiento, C. Fei, X. Zhang, and H. Wang, Effect of composition on the spin relaxation of lead halide perovskites, *J. Phys. Chem. Lett.* **11**, 1502 (2020).
- [68] J. Chen, K. Wu, W. Hu, and J. Yang, Tunable Rashba spin splitting in two-dimensional polar perovskites, *J. Phys. Chem. Lett.* **12**, 1932 (2021).
- [69] L. Leppert, S. E. Reyes-Lillo, and J. B. Neaton, Electric field- and strain-induced Rashba effect in hybrid halide perovskites, *J. Phys. Chem. Lett.* **7**, 3683 (2016).
- [70] V. V. Belykh, D. R. Yakovlev, M. M. Glazov, P. S. Grigoryev, M. Hussain, J. Rautert, D. N. Dirin, M. V. Kovalenko, and M. Bayer, Coherent spin dynamics of electrons and holes in CsPbBr<sub>3</sub> perovskite crystals, *Nat. Commun.* **10**, 673 (2019).
- [71] M. Li, L. Li, R. Mukherjee, K. Wang, Q. Liu, Q. Zou, H. Xu, J. Tisdale, Z. Gai, I. N. Ivanov *et al.*, Magnetodielectric response from spin-orbital interaction occurring at interface of ferromagnetic Co and organometal halide perovskite layers via Rashba effect, *Adv. Mater.* **29**, 1603667 (2017).
- [72] C. Zhang, D. Sun, C. X. Sheng, Y. X. Zhai, K. Mielczarek, A. Zakhidov, and Z. V. Vardeny, Magnetic field effects in hybrid perovskite devices, *Nat. Phys.* **11**, 427 (2015).
- [73] J. Wang, C. Zhang, H. Liu, R. McLaughlin, Y. Zhai, S. R. Vardeny, X. Liu, S. McGill, D. Semenov, H. Guo *et al.*, Spin-optoelectronic devices based on hybrid organic-inorganic trihalide perovskites, *Nat. Commun.* **10**, 129 (2019).
- [74] J. Wang, C. Zhang, H. Liu, X. Liu, H. Guo, D. Sun, and Z. V. Vardeny, Tunable spin characteristic properties in spin valve devices based on hybrid organic-inorganic perovskites, *Adv. Mater.* **31**, 1904059 (2019).
- [75] K. Wang, Q. Yang, J. Duan, C. Zhang, F. Zhao, H. Yu, and B. Hu, Spin-polarized electronic transport through ferromagnet/organic-inorganic hybrid perovskite spinterfaces at room temperature, *Adv. Mater. Interfaces* **6**, 1900718 (2019).
- [76] A. Filippetti, P. Wadhwa, C. Caddeo, and A. Mattoni, A promising outlook on the development of lead halide perovskites as spin-orbitronic materials, *Appl. Phys. Lett.* **121**, 200501 (2022).
- [77] D. Sun, C. Zhang, M. Kavand, J. Wang, H. Malissa, H. Liu, H. Popli, J. Singh, S. R. Vardeny, W. Zhang *et al.*, Surface-enhanced spin current to charge current conversion efficiency in CH<sub>3</sub>NH<sub>3</sub>PbBr<sub>3</sub>-based devices, *J. Chem. Phys.* **151**, 174709 (2019).
- [78] Y. Zhai, S. Baniya, C. Zhang, J. Li, P. Haney, C.-X. Sheng, E. Ehrenfreund, and Z. V. Vardeny, Giant Rashba splitting in 2D organic-inorganic halide perovskites measured by transient spectroscopies, *Sci. Adv.* **3**, e1700704 (2017).
- [79] X. Liu, A. Chanana, U. Huynh, F. Xue, P. Haney, S. Blair, X. Jiang, and Z. V. Vardeny, Circular photogalvanic spectroscopy of Rashba splitting in 2D hybrid organic-inorganic perovskite multiple quantum wells, *Nat. Commun.* **11**, 323 (2020).
- [80] I. H. Park, Q. Zhang, K. C. Kwon, Z. Zhu, W. Yu, K. Leng, D. Giovanni, H. S. Choi, I. Abdelwahab, Q. H. Xu *et al.*, Ferroelectricity and Rashba effect in a two-dimensional Dion-Jacobson hybrid organic-inorganic perovskite, *J. Am. Chem. Soc.* **141**, 15972 (2019).
- [81] M. T. Pham, E. Amerling, H. M. Luong, H. T. Pham, G. K. Larsen, L. Whittaker-Brooks, and T. D. Nguyen, Origin of Rashba spin-orbit coupling in 2D and 3D lead iodide perovskites, *Sci. Rep.* **10**, 4964 (2020).
- [82] S. B. Todd, D. B. Riley, A. Binai-Motlagh, C. Clegg, A. Ramachandran, S. A. March, J. M. Hoffman, I. G. Hill, C. C. Stoumpos, M. G. Kanatzidis *et al.*, Detection of Rashba spin splitting in 2D organic-inorganic perovskite via precessional carrier spin relaxation, *APL Mater.* **7**, 081116 (2019).
- [83] F. Wang, H. Gao, C. de Graaf, J. M. Poblet, B. J. Campbell, and A. Stroppa, Switchable Rashba anisotropy in layered hybrid organic-inorganic perovskite by hybrid improper ferroelectricity, *npj Comput. Mater.* **6**, 183 (2020).
- [84] H. Wang, L. Liang, J. Li, W. Yao, and D. Li, Enhanced Rashba indirect exciton emission in 2D Dion-Jacobson perovskite microplates via efficient photon recycling, *Adv. Optical Mater.* **10**, 2102103 (2021).
- [85] J. Yin, P. Maity, L. Xu, A. M. El-Zohry, H. Li, O. M. Bakr, J.-L. Brédas, and O. F. Mohammed, Layer-dependent Rashba band splitting in 2D hybrid perovskites, *Chem. Mater.* **30**, 8538 (2018).
- [86] J. Yin, R. Naphade, P. Maity, L. Gutierrez-Arzaluz, D. Almalawi, I. S. Roqan, J. L. Bredas, O. M. Bakr, and O. F. Mohammed, Manipulation of hot carrier cooling dynamics in two-dimensional Dion-Jacobson hybrid perovskites via Rashba band splitting, *Nat. Commun.* **12**, 3995 (2021).
- [87] B. Zhou, L. Liang, J. Ma, J. Li, W. Li, Z. Liu, H. Li, R. Chen, and D. Li, Thermally assisted Rashba splitting and circular photogalvanic effect in aqueously synthesized 2D Dion-Jacobson perovskite crystals, *Nano Lett.* **21**, 4584 (2021).
- [88] S. Varotto, L. Nessi, S. Cecchi, J. Sławińska, P. Noël, S. Petrò, F. Fagiani, A. Novati, M. Cantoni, D. Petti *et al.*, Room-temperature ferroelectric switching of spin-to-charge conversion in GeTe, *Nat. Electron.* **4**, 740 (2021).
- [89] K. Leng, R. Li, S. P. Lau, and K. P. Loh, Ferroelectricity and Rashba effect in 2D organic-inorganic hybrid perovskites, *Trends Chem.* **3**, 716 (2021).
- [90] P. Noel, F. Trier, L. M. Vicente Arche, J. Brehin, D. C. Vaz, V. Garcia, S. Fusil, A. Barthelemy, L. Vila, M. Bibes *et al.*, Non-volatile electric control of spin-charge conversion in a SrTiO<sub>3</sub> Rashba system, *Nature (London)* **580**, 483 (2020).
- [91] R. Yang, In-memory computing with ferroelectrics, *Nat. Electron.* **3**, 237 (2020).
- [92] L. Mao, W. Ke, L. Pedesseau, Y. Wu, C. Katan, J. Even, M. R. Wasielewski, C. C. Stoumpos, and M. G. Kanatzidis, Hybrid Dion-Jacobson 2D lead iodide perovskites, *J. Am. Chem. Soc.* **140**, 3775 (2018).
- [93] G. Kresse and J. Furthmüller, Efficient iterative schemes for *ab initio* total-energy calculations using a plane-wave basis set, *Phys. Rev. B* **54**, 11169 (1996).
- [94] J. P. Perdew, K. Burke, and M. Ernzerhof, Generalized Gradient Approximation Made Simple, *Phys. Rev. Lett.* **77**, 3865 (1996).
- [95] U. Herath, P. Tavazde, X. He, E. Bousquet, S. Singh, F. Muñoz, and A. H. Romero, PyProcar: A Python library for electronic structure pre/post-processing, *Comput. Phys. Commun.* **251**, 107080 (2020).
- [96] D. M. Bylander and L. Kleinman, Energy fluctuations induced by the nose thermostat, *Phys. Rev. B* **46**, 13756 (1992).

- [97] See Supplemental Material at <http://link.aps.org/supplemental/10.1103/PhysRevB.107.155436> for additional data and analyses, which includes Refs. [92,98,99].
- [98] R. Uehara, S. Matsushita, A. Nakajima, and T. Isobe, Effect of tin substitution on the chemical composition and thermal expansion properties of  $Zr_2SP_2O_{12}$ , *J. Asian Ceram. Soc.* **9**, 1194 (2021).
- [99] K. Robinson, G. V. Gibbs, and P. H. Ribbe, Quadratic elongation a quantitative measure of distortion in coordination polyhedra, *Science* **172**, 567 (1971).
- [100] T. Wang, B. Daiber, J. M. Frost, S. A. Mann, E. C. Garnett, A. Walsh, and B. Ehrler, Indirect to direct bandgap transition in methylammonium lead halide perovskite, *Energy Environ. Sci.* **10**, 509 (2017).
- [101] B. Wu, H. Yuan, Q. Xu, J. A. Steele, D. Giovanni, P. Puech, J. Fu, Y. F. Ng, N. F. Jamaludin, A. Solanki *et al.*, Indirect tail states formation by thermal-induced polar fluctuations in halide perovskites, *Nat. Commun.* **10**, 484 (2019).
- [102] E. M. Hutter, M. C. Gelvez-Rueda, A. Osherov, V. Bulovic, F. C. Grozema, S. D. Stranks, and T. J. Savenije, Direct-indirect character of the bandgap in methylammonium lead iodide perovskite, *Nat. Mater.* **16**, 115 (2017).
- [103] F. Zheng, L. Z. Tan, S. Liu, and A. M. Rappe, Rashba spin-orbit coupling enhanced carrier lifetime in  $CH_3NH_3PbI_3$ , *Nano Lett.* **15**, 7794 (2015).
- [104] J. Ma, C. Fang, C. Chen, L. Jin, J. Wang, S. Wang, J. Tang, and D. Li, Chiral 2D perovskites with a high degree of circularly polarized photoluminescence, *ACS Nano* **13**, 3659 (2019).
- [105] H. Zeng, J. Dai, W. Yao, D. Xiao, and X. Cui, Valley polarization in  $MoS_2$  monolayers by optical pumping, *Nat. Nanotechnol.* **7**, 490 (2012).
- [106] A. D. Wright, C. Verdi, R. L. Milot, G. E. Eperon, M. A. Perez-Osorio, H. J. Snaith, F. Giustino, M. B. Johnston, and L. M. Herz, Electron-phonon coupling in hybrid lead halide perovskites, *Nat. Commun.* **7**, 11755 (2016).
- [107] T. Etienne, E. Mosconi, and F. De Angelis, Dynamical origin of the Rashba effect in organohalide lead perovskites: A key to suppressed carrier recombination in perovskite solar cells? *J. Phys. Chem. Lett.* **7**, 1638 (2016).
- [108] E. Mosconi, T. Etienne, and F. De Angelis, Rashba band splitting in organohalide lead perovskites: Bulk and surface effects, *J. Phys. Chem. Lett.* **8**, 2247 (2017).
- [109] Y. A. Bychkov and E. I. Rashba, Properties of a 2D electron gas with lifted spectral degeneracy, *JETP Lett.* **39**, 78 (1984).
- [110] V. Sunko, H. Rosner, P. Kushwaha, S. Khim, F. Mazzola, L. Bawden, O. J. Clark, J. M. Riley, D. Kasinathan, M. W. Haverkort *et al.*, Maximal Rashba-like spin splitting via kinetic-energy-coupled inversion-symmetry breaking, *Nature (London)* **549**, 492 (2017).
- [111] J. Prempfer, M. Trautmann, J. Henk, and P. Bruno, Spin-orbit splitting in an anisotropic two-dimensional electron gas, *Phys. Rev. B* **76**, 073310 (2007).
- [112] H. Y. Yang, C. Huang, H. Ochoa, and M. A. Cazalilla, Extrinsic spin Hall effect from anisotropic Rashba spin-orbit coupling in graphene, *Phys. Rev. B* **93**, 085418 (2016).
- [113] M. El-Batanouny, in *Advanced Quantum Condensed Matter Physics: One-Body, Many-Body, and Topological Perspectives* (Cambridge University, Cambridge, 2020).
- [114] J. Chen, K. Wu, H. Ma, W. Hu, and J. Yang, Tunable Rashba spin splitting in Janus transition-metal dichalcogenide monolayers via charge doping, *RSC Adv.* **10**, 6388 (2020).
- [115] P. A. L. Sino, L. Y. Feng, R. A. B. Villaos, H. N. Cruzado, Z. Q. Huang, C. H. Hsu, and F. C. Chuang, Anisotropic Rashba splitting in Pt-based Janus monolayers  $PtXY$  ( $X, Y = S, Se, or Te$ ), *Nanoscale Adv.* **3**, 6608 (2021).